1 Title: Discovery of M Protease inhibitors encoded by SARS-CoV-2

2 Running title: GC376 is potent inhibitor of SARS-CoV-2 M^{pro}.

3 Hui-Chen Hung[a], Yi-Yu Ke[a], Sheng Yu Huang[d], Peng-Nien Huang[d,e], Yu-An Kung[d,e], Teng-
4 Yuan Chang[a], Kuei-Jung Yen[a], Tzu-Ting Peng[c], Shao-En Chang[a], , Chin-Ting Huang[a],Ya-Ru
5 Tsai[a], Szu-Huei Wu[a], Shiow-Ju Lee[a], Jiunn-Horng Lin[c], Bing-Sin Liu[g], Wang-Chou Sung[g],
6 Shin-Ru Shih[d,f,]*, Chiung-Tong Chen[a,]*, John Tsu-An Hsu[a,b,]*

7

8 [a]*Institute of Biotechnology and Pharmaceutical Research, National Health Research Institutes,*
9 *Miaoli, Taiwan*

10 [b]*Department of Biological Science and Technology, National Chiao Tung University, Hsinchu,*
11 *Taiwan*

12 [c]*Department of Animal Technology Laboratories, Agricultural Technology Research Institute*
13 *(ATRI), Miaoli, Taiwan*

14 [d]*Research Center for Emerging Viral Infections, Chang Gung University, Taoyuan, Taiwan.*

15 [e]*Division of Infectious Diseases, Department of Pediatrics, Linkou Chang Gung Memorial*
16 *Hospital, Taoyuan, Taiwan.*

17 [f]*Department of Laboratory Medicine, Linkou Chang Gung Memorial Hospital, Taoyuan, Taiwan.*

[g]*National Institute of Infectious Diseases and Vaccinology, National Health Research Institutes, Miaoli, Taiwan*

*Corresponding authors

Research Center for Emerging Viral Infections, Chang Gung University, Taoyuan, Taiwan. Tel: 886-32-118800 ext 5794

Shin-Ru Shih, srshih@*mail*.cgu.edu.tw

Institute of Biotechnology and Pharmaceutical Research, National Health Research Institutes, Miaoli, Taiwan. Tel: 886-37-246166 ext 35701

Chiung-Tong Chen, ctchen@nhri.edu.tw

Institute of Biotechnology and Pharmaceutical Research, National Health Research Institutes, Miaoli, Taiwan. Tel: 886-37-246166 ext 35717

John Tsu-An Hsu, tsuanhsu@nhri.edu.tw

Shin-Ru Shih, Chiung-Tong Chen, John Tsu-An Hsu contributed equally to this work.

35 **Abbreviations**

36 M^{pro}, Main Protease**,** Severe Acute Respiratory Syndrome Coronavirus-2, SARS-CoV-2,Severe
37 Acute Respiratory Syndrome, SARS, Middle East respiratory syndrome, MERS, novel
38 coronavirus disease-2019, COVID-19, feline infectious peritonitis virus, FIPV, a half-maximum
39 effective concentration, EC_{50}, inhibitory concentrations, IC_{50}, human immunodeficiency virus,
40 HIV, Dimethyl sulfoxide, DMSO, fluorescence resonance energy transfer, FRET, cytopathic
41 effect, CPE, 50 % tissue culture infectious dose, TCID50, cytotoxic concentration, $CC_{50,}$
42 interferon, IFN,

Abstract:

The COVID-19 pandemic caused by SARS-CoV-2 is a health threat worldwide. Viral main protease (M^{pro}, also called 3C-like protease, $3CL^{pro}$) is a therapeutic target for drug discovery. Herein, we report that GC376, a broad-spectrum inhibitor targeting M^{pro} in the picornavirus-like supercluster, is potent inhibitor for the M^{pro} encoded by SARS-CoV-2 with half-maximum inhibitory concentration (IC_{50}) of 26.4±1.1 nM. In this study, we also show that GC376 inhibits SARS-CoV-2 replication with a half-maximum effective concentration (EC_{50}) of 0.91±0.03 μM. Only a small portion of SARS-CoV-2-M^{pro} was covalently modified in the excess of GC376 as evaluated by mass spectrometry analysis; indicating that improved inhibitors are needed. Subsequently, molecular docking analysis revealing the recognition and binding groups of GC376 within the active site of SARS-CoV-2 M^{pro} provides important new information for the optimization of GC376. Given that sufficient safety and efficacy data are available for GC376 as an investigational veterinary drug, expedited development of GC376, or its optimized analogues, for treatment of SARS-CoV-2 infection in human is recommended.

Keywords: COVID-19, SARS-CoV-2, M^{pro} , Antiviral research, GC376

1. Introduction

Coronavirus infection in humans and other animals has resulted in a variety of highly prevalent and serious diseases, including severe acute respiratory syndrome (SARS) and Middle East respiratory syndrome (MERS). Beginning in Wuhan city of China in late 2019, the novel coronavirus disease-2019 (COVID-19) caused by Severe Acute Respiratory Syndrome Coronavirus-2 (SARS-CoV-2) has spread to the whole world (1, 2). Similar to SARS-CoV and MERS-CoV, the newly identified SARS-CoV-2 also belongs to the genus *Betacoronavirus* with zoonotic origin (3, 4). SARS-CoV-2 cause common symptoms including fever, cough, and shortness of breath. Complications may include pneumonia and acute respiratory distress syndrome (5, 6).

The genome of COVID-19 virus consists of about 30,000 nucleotides; its replicase gene encodes two overlapping polyproteins, pp1a and pp1ab, which are needed for virus replication and transcription. The functional viral proteins are released from the polypeptide through proteolysis, mainly by main protease (M^{pro}), which is also referred as 3C-like protease (7). M^{pro} can digest at least 11 conserved sites within viral polyproteins. Viral M^{pro} has been considered as therapeutic targets for development of effective antiviral treatment (8). Among all the mature structural or non-structural proteins in SARS-CoV-2, M^{pro} is the most conserved target region within the whole viral genome (9). Due to the severity of SARS-CoV-2 infection, it is important to emphasize drug discovery for SARS-CoV-2 based on existing drugs for immediate uses or expedited development timeline.

We have previously discovered several small molecule inhibitors for SARS-CoV during the SARS outbreak in 2003 (10). The M^{pro} encoded by SARS-CoV-2 represents a key target for anti-

SARS-CoV-2 strategies. However, to date, promising SARS-CoV-2 M^{pro} protease inhibitor has been lacking. Herein, we established the SARS-CoV-2 M^{pro} protease fluorescence-based assay to screen for potential inhibitors. Furthermore, molecular modeling studies were carried out to further demonstrate the interaction of M^{pro} with GC376. GC376 or its optimized analogues holds great promise to be developed in human with SARS-CoV-2 infection, alone or together with other antiviral drugs.

Antimicrobial Agents and Chemotherapy

2. Materials and Methods

2.1 Drugs and Reagents

The test compounds were mainly from Selleck and MedChemExpress. Several in-house collected compounds including human immunodeficiency virus (HIV) protease inhibitors, GC376 and natural products were also included for screening as M^{pro} inhibitors. GC376 was purchased from Biosynth Carbosynth®. It was dissolved in dimethyl sulfoxide (DMSO) as a 10 mM stock solution and stored at −20°C. The fluorogenic substrate peptide-Dabcyl-KTSAVLQSGFRKME-Edans utilized in the fluorescence resonance energy transfer (FRET) assay for M^{pro} were obtained from Genesis Biotechnology Inc..

2.2 Expression and purification of 3C-like proteases (M^{pro})

To express the M protease (M^{pro}) from SAR-CoV-2 and FIPV, cDNA's encoding the genes as deduced from Wuhan-Hu-1 strain (NC_045512.2) and WSU-79/1146 strain (AAY32595.1) were optimized for codon preference in *E. coli*, respectively. The amino acid sequence of the SARS-CoV-2 M^{pro} is shown in Fig. S1(A). The synthetic cDNA (BIO BASIC, Canada) encoded the M^{pro} was respectively inserted into expression plasmid vector pGEX-4T-1 (GE Health Care) using *BamH* I and *Xho* I restriction enzyme cutting sites (Fig. S1(b)), resulting in a factor Xa cleavage site, an expanded multiple cloning site, and ampicillin resistant gene was used as a selection marker.

The recombinant plasmid was transfected into Rosetta2 (DE3) pLysS strain (Novagen), an *E. coli* host, and the overnight culture in LB medium was refreshed to an OD600 of 0.8 at 37°C, then induced with 1 mM IPTG for 5 hours at 25°C. The cells were harvested by

centrifugation at 4°C (6,000 rpm, 10 min) followe by sonication in lysis buffer containing 1× Phosphate buffered saline (137 mM NaCl, 10 mM Phosphate, 2.7 mM KCl, *p*H=7.4), 0.1% Triton X100. The GST-M^{pro} fusion protease was purified by Glutathione Sepharose 4 Fast Flow (GE Healthcare) with purification buffer (50 mM Tris, *p*H=8.0, 10 mM glutathione). The purified GST-M^{pro} fusion protease was changed to factor Xa digestion buffer (20 mM Tris, *p*H=6.6, 50 mM NaCl, 1 mM $CaCl_2$), and digested with factor Xa at 20°C overnight. The digested GST-M^{pro} was reloaded into glutathione sepharose column to collect the flow-through for separation of M^{pro}. SDS-PAGE analysis shows that the M^{pro} is purified with approximately 95% purity. The M^{pro} was changed to storage buffer (50 mM Tris, 100 mM NaCl, 1 mM KCl, 1mM $CaCl_2$, 25% glycerol) using Amicon (10K, Millipore), aliquoted, and stored at -20°C.

2.3 Protease activity assay

The protease assays were performed in 96-well black flat-bottomed microtiter plates (Greiner Bio one, Germany) with a final volume of 100 µL. SARS-CoV-2 M^{pro} recombinant protease, at a final concentration of 20 nM, was pre-incubated for 10 min at room temperature (RT) with compounds at different concentrations in the assay buffer (20 mM HEPES *p*H=6.0, 0.4 mM EDTA, 1 mM DTT, 1% glycerol). The FRET substrate, Dabcyl-KTSAVLQSGFRKME-Edans, was then added at a final concentration of 10 µM to the enzymatic reaction for 30 min at RT. The readouts for the same compound concentrations with the substrate without M^{pro} enzyme were measured as a blank. The fluorescence signals (excitation/emission: 355 nm/460 nm) of released Edans were measured using a fluorometer (VICTOR2, PerkinElmer). The results were plotted as dose-inhibition curves using non-linear regression with a variable slope to determine the IC_{50} values of inhibitor compounds (with GraphPad Prism 5.0). *Ki* measurements were

performed with various substrate concentrations of 5, 10, 20, 40 μM and a range of inhibitor concentrations (0, 8, 40, 200, 1000 nM) in a reaction mixture containing 20 nM M^{pro} at 37°C for 30 min. The *Ki* value was computed using GraphPad Prism 5.0 software by nonlinear regression of competitive enzyme kinetics.

2.4 Antiviral assay and Cytotoxicity assay

To examine the anti-SARS-CoV-2 activity of positive compounds identified in the M^{pro} activity assay, $TCID_{50}$ (50% tissue culture infectious dose) was performed using two-fold serial dilutions of hit compounds starting from 50 μM. In brief, each well in 96-well tissue culture plate was seeded with 200 μL of 1.15×10^5 Vero E6 cells/mL in MEM with 10% FBS. After cells were incubated for 18–24 h at 37°C, SARS-CoV-2/human/TWN/CGMH-CGU-01/2020 virus at $100\times TCID_{50}$ per well mixed with different concentrations of GC376. After 5 days, cells were fixed with formaldehyde and stained with 0.1% crystal violet as described previously (11). The concentration required for the tested compound to reduce the cytopathic effect (CPE) of the virus by 50% (the 50% effective concentration; EC_{50}) was determined. IC_{50} was calculated using GraphPad Prism 6 to assess inhibition percentage at different inhibitor concentrations. To estimate the safety profile, the *in vitro* cytotoxicity study of GC376 was performed. We used MTT assay to investigate the cytotoxicity of these compounds on Vero E6 cells. The half-cytotoxic concentration (CC_{50}) values were calculated from the inhibitory percentages of GC376 at various concentrations on the viability of the cells.

2.5 Molecular Modeling

The docking of compounds into the binding sites of the SARS-CoV-2-M^{pro} (PDB ID: 6LU7) (12) or M^{pro} of feline infectious peritonitis virus, FIPV-M^{pro} (PDB ID: 4ZRO) (6) was explored

using BIOVIA 2018/Liganfit program (BIOVIA, Inc., San Diego, CA). The detailed method of Ligandfit has been described (13) To illustrate the binding interactions, GC376 was docked into the binding site. The binding pocket was identified from the MERS and GC376 co-crystal structure (PDB ID: 5WKJ) (14). The forcefield for calculating ligand-receptor interaction energies employed the piecewise linear potential 1 (PLP1). The rectangular grid was set as 0.5 Å spacing and the extension from Site was set as 8 Å. The number of docking poses was set as 50 with default parameters. The docking root mean square (RMS) threshold for ligand-site matching was set as 5 Å. The method of steepest descent for the rigid-body minimization during pose docking was used. The covalent docking calculation was performed using the two-point attractor method by the AutoDock Tools (version 1.5.6) as described (15). The decision of the best pose was based on the similar conformations of the MERS complex co-crystal structure.

2.6 Molecular weight analysis using MS

The premixed GC376 compound (1µl, 10 mM in DMSO) and the SARS-CoV-2-M^{pro} (5µl, 2.5mg/ml) was incubated at 25℃ for 30 mins. Subsequently, 10 µL of reaction mixture was transferred into 40µl of the infusion solution (50% Acentonitrile in 0.1% Formic acid) for measuring the molecular weight using QTOF mass spectrometer. (G1, WATERS) through the direct infusion model. The ion signal (m/z) was acquired in positive-ion mode with a capillary temperature of 100 °C, electrospray voltage of 2800 V in the scan range from 800 to 2500 m/z.

The Mass deconvolution was performed using Waters MassLynx (V4.1) software using the MaxEnt 1 program with the of half height 0.1 Da, and the Maximum number of interaction of 100.

3. Results

3.1 FRET-based Screening Assays

The M^{pro} encoded by these two coronaviruses differ in only 12 amino acid residues. According to our previous experience during the SARS outbreak, SARS-CoV-2 M^{pro} was expressed as an GST fusion protein in *E. coli* BL21 (DE3)(16, 17). The GST fusion protein was purified by glutathione affinity chromatography. The fusion protein was cleaved by Factor Xa, resulting in the generation of a prominent protein band with an apparent molecular mass of 35 kDa and obtained the mature SARS-CoV-2 M^{pro} (Fig. S1(c)).

Purified M^{pro} proteins were checked for the proteolytic activity of cleaving the Edans-KTSAVLQSGFRKME-Dabcyl substrate (Fig. S2(a)). The purified enzyme was assayed using the FRET technique as described in Materials and Methods. The performance of FRET assay was assessed and the signal-to-noise ratio was determined to be >20 (Fig. S2(b)). The Z-factor value for the assay was 0.9, which corresponds to a valid screening system. The M^{pro} of FIPV was prepared similarly. The same fluorogenic substrate, Edans-KTSAVLQSGFRKME-Dabcyl, was equally applicable in activity assessment for FIPV-M^{pro}.

3.2 Inhibitory activity of SARS-CoV-2 M^{pro} by Zinc ion, GC376 and lopinavir

In this study, based on the SARS-CoV-2-M^{pro} activity assay, we screened a collection of protease inhibitors such as reported M^{pro} inhibitors for relevant viruses and clinically approved HIV protease inhibitors. At 10 μM, GC376 (Fig. 1A), a broad-spectrum antiviral protease inhibitor used to treat cats with FIPV infection (18), showed complete inhibition of SARS-CoV-2 M^{pro} activity. Since GC376 was well characterized for its inhibition of M^{pro} encoded by FIPV,

we conducted head-to-head comparison for the inhibitory activity of GC376 on SARS-CoV-2-M^{pro} and FIPV-M^{pro}. SARS-CoV-2 and SARS-CoV share high identity in amino acid sequences (Fig. S3(a)), whereas SARS-CoV-2-M^{pro} and FIPV-M^{pro} share 45% identity in amino acid sequence (Fig S3(b)). These two viral proteases also share similar folding and crystal structure (12, 19). In this study, we found that GC376 is an extremely potent inhibitor for the M^{pro} encoded by SARS-CoV-2 with a half-maximum inhibitory concentration (IC_{50}) of 26.4 ± 1.1 nM (Fig. 1B). Subsequent analysis showed that GC376 is a competitive inhibitor for the M^{pro} from SARS-CoV-2 with a binding constant *Ki* of 12 ± 1.4 nM (Fig. 1C). In contrast, the IC_{50} and *Ki* of GC376 toward FIPV-M^{pro} are 118.9 ± 1.1 nM and 42.5 ± 2.9 nM, respectively (Fig S4(a) and (b)).

To examine whether covalent adduct is formed, SARS-CoV-2 M^{pro} incubated with GC376 was subject to mass spectrometry analysis in accordance to a method as described previously. Indeed, a gain of 403.2 dalton in mass was observed in new peaks from the GC376-incubated SARS-CoV-2 M^{pro} indicating the same mechanism for adduct formation as described (18) (results not shown). Through the mass spectrometry analysis, a new MS peak was observed with the mass value of 34,194.0 (Da), which is equal to the dehydrogen molecular weight of M protease (33,790.8); reflecting conjugation with only one GC376 molecule. Even in the excess of GC376, only 30% of the M^{pro} was conjugated based on the peak intensity. With the X-ray (7BRR, released date: 2020-05-13) and the MS analysis performed in this study, it is evident that GC376 forms a covalent bond with Cys145 of M protease (M^{pro}). That only a small portion of SARS-CoV-2-M^{pro} was covalently modified, in the 25:1 molar excess of GC376, indicates that improved inhibitors are needed.

All the HIV protease inhibitors including lopinavir and ritonavir showed no inhibitory activity at 20 μM, reflecting the fact that no benefit was observed with lopinavir–ritonavir treatment in patients with severe Covid-19 (20). Since Zn^{2+} was shown to inhibit $3CL^{pro}$ encoded by SARS-CoV (15), $ZnCl_2$ and $ZnSO_4$ were evaluated for their activity on SARS-CoV-2 M^{pro} in this study. Zinc salts are shown to completely inhibit the activity of SARS-CoV-2 M^{pro} at micro molar level (data not shown).

3.3 Antiviral effects of GC376 on the replication of SARS-CoV-2 in cell culture

To confirm that the GC376 inhibited SARS-CoV-2 replication and cellular toxicity in cell culture, GC376 was tested for inhibition of SARS-CoV-2 infection in Vero E6 cells with 100 $TCID_{50}$ per well in 96-well plate. SARS-CoV-2-infected cells were treated with increasing concentrations of GC376 and protection from CPE was visually observed. GC376 dose-dependently showed reduction of viral cytopathic effect (Fig. S5). After the cells were stained with crystal violet and measured at O.D. 570 nm (Fig. 2A). The results showed that GC376 inhibited SARS-CoV-2 infection with an EC_{50} of 0.91 ± 0.03 μM (Fig. 2B). GC376 exhibited a broad-spectrum antiviral activity against several coronaviruses in various cell lines (18). To evaluate whether GC376 was cytotoxic to cells, Vero E6 cells were treated with different concentrations of GC376 up to 100 μM, and cell viability was determined using MTT assay. We found that GC376 did not show cytotoxicity in Vero E6 cells up to 100 μM (Fig. 2B). Hence, we concluded that the selectivity index (SI) of GC376 was >> 114.

Antimicrobial Agents and Chemotherapy

3.4 Molecular Docking

To inform lead optimization efforts starting from GC376, *in silico* calculations to correlate IC_{50} and *Ki* into binding energy between GC376 and M^{pro} is attempted in accordance to, in part, our previous work (21-23). In our calculation, the free binding energy of GC376 with SARS-CoV-2-M^{pro} and FIPV-M^{pro} are -51.59 Kcal/mol and -32.42 Kcal/mol, respectively. As shown in Figures 3A and 3B, upon removal of the bisulfite group, the compound is converted to an aldehyde form, giving rise to a covalent bond with catalytic Cys145. This result is in congruence with the co-crystal structure of GC376 and MERS-M^{pro} where GC376 forms a covalent bond with Cys148 (11). In Figure 3C, the amino acid residues on the inner surface of the substrate binding sites within the FIPV-M^{pro} and SARS-CoV-2-M^{pro} are well conserved. Only two sites of amino acid residues are different between the two M^{pro} binding pocket. In SARS-CoV-2, the Gln189 on the surface of binding pocket of SARS-CoV-2-M^{pro} supports a H-bond with the carbamate moiety of GC376. On the contrary, this H-bond cannot be formed because the counterpart residue in FIPV-M^{pro} is Pro188, rather than Gln. It appears that due to the covalent binding with Cys145 and hydrogen binding with Gln189 within substrate binding pocket of SARS-CoV-2-M^{pro}, GC376 was induced to bind more snugly into the pocket through a strong H-bond network with Phe140, Gly143, Ser144, Cys145, His163, His164, Glu166, and Gln189 (Figure 3A). On the contrary, GC376 only forms a weaker H-bond network with Gly142, His162, and Glu165 (Figure 3B). The other different site is Ser144 in SARS-CoV-2-M^{pro} and Thr143 in FIPV-M^{pro}. This difference has little influence on the binding network. The root-mean-square deviation (RMSD) between the two docking conformations of GC376/SARS-CoV-2 and GC376/FIPV is 1.16 Å. Importantly, our *in silico* prediction has informed potential direction to improve GC376 with respective to its potency and further drug-like properties. With the docking

analyses, GC376 may be improved by replacing the benzene group by H-bond donors to interact with Glu166. The other alternative for improvement on binding potency is to replace the isobutyl group with moieties of less bulky hydrophobic group so as to form interactions with Met49 (Figure 3C). Hussey RJ. have reported that the Michael acceptor inhibitor, acetyl-Glu-Phe-Gln-Leu-Gln-CH=CHCOO-, will form a covalent bond with catalytic Cys139 in Norovirus $3CL^{pro}$ (24), suggesting an alternative revenue for optimization of GC376. After the submission of this manuscript, the crystal structure of the 3CL protease complexed with GC376 (7BRR, released date: 2020-05-13) became available in Protein Data Base (PDB). By comparing the co-crystal X-ray with our docked M^{pro}-GC376 model based on 6LU7, the RMSD is 0.74; indicating that the in silico docking approach employed in this study adequately predicted the real complexed structure before its availability. In Fig S6, the modeled conformation is shown in green color and aligned to the X-ray result in pink.

4. Discussion

To date, no proven effective therapy has been shown to be effective for SARS-CoV-2 infection (9). As of the submission date of this manuscript, the once promising medicines including remdesivir and hydroxychloroquine are facing challenges after more stringently controlled observations and trials (25, 26). When coronaviruses are replicating inside cells, cellular innate immunity was shown to be compromised by M^{pro} (27). We have previously shown that the compromised interferon (IFN)-mediated antiviral mechanism by viral $3C^{pro}$ of enterovirus 71 can be rescued by effective protease inhibitor (28). Thus, effective inhibition on viral protease not only could restrict virus replication, but also would prevent interruption of the antiviral IFN-pathway.

We also found that GC376 is a promising M^{pro} inhibitor for SARS-CoV-2. GC376 is a dipeptidyl bisulfite adduct salt with excellent inhibitory activity on several picornaviruses and coronaviruses (18, 29, 30). Administration of GC376 leads to a full recovery in laboratory cats with FIPV infection, a highly fatal feline disease (31). Kim Y. (2016) also studied pharmacokinetic properties and safety of GC376 in laboratory cats. In their safety study on GC376, no adverse effects was observed and no changes in clinical lab parameters was reported in cats subcutaneously given GC376 at 10 mg/kg/dose, twice a day, for 4 weeks (31). In this safety study, the plasma drug concentrations were shown to be remained slightly above 1,000 ng/mL (i.e., ~2,000 nM as the M.W. of GC376 is 507.53) that was well above the concentrations needed for effective inhibition of SARS-CoV-2 as observed in this study. Therefore, the existing pharmacology and efficacy data for GC376 as an investigational drug in cat with FIPV infection

297 encourage studying proof of principle in COVID-19 patients followed by *in vitro* and *in vivo*
298 antiviral activity of GC376, or further optimized analogues.

299

300 **Conflicts of interest**

301 The authors declare that they have no competing interests.

302

Acknowledgments:

This work was financially supported by a special government fund to tackle the COVID-19 pandemic from the Ministry of Health and Welfare, Taiwan and a 5-year grant for the Research Center for Emerging Viral Infections (Chang Gung University) from The Featured Areas Research Center Program within the framework of the Higher Education Sprout Project by the Ministry of Education (MOE) in Taiwan, the Ministry of Science and Technology (MOST). The team also thanks Ms. Huai-Tzu Chang for coordination and facilitation on the project.

References

1. Wu D, Wu T, Liu Q, Yang Z. 2020. The SARS-CoV-2 outbreak: what we know. Int J Infect Dis doi:10.1016/j.ijid.2020.03.004.
2. Coronaviridae Study Group of the International Committee on Taxonomy of V. 2020. The species Severe acute respiratory syndrome-related coronavirus: classifying 2019-nCoV and naming it SARS-CoV-2. Nat Microbiol 5:536-544.
3. Hu B, Ge X, Wang LF, Shi Z. 2015. Bat origin of human coronaviruses. Virol J 12:221.
4. Zhou P, Yang XL, Wang XG, Hu B, Zhang L, Zhang W, Si HR, Zhu Y, Li B, Huang CL, Chen HD, Chen J, Luo Y, Guo H, Jiang RD, Liu MQ, Chen Y, Shen XR, Wang X, Zheng XS, Zhao K, Chen QJ, Deng F, Liu LL, Yan B, Zhan FX, Wang YY, Xiao GF, Shi ZL. 2020. A pneumonia outbreak associated with a new coronavirus of probable bat origin. Nature 579:270-273.
5. Wolfel R, Corman VM, Guggemos W, Seilmaier M, Zange S, Muller MA, Niemeyer D, Jones TC, Vollmar P, Rothe C, Hoelscher M, Bleicker T, Brunink S, Schneider J, Ehmann R, Zwirglmaier K, Drosten C, Wendtner C. 2020. Virological assessment of hospitalized patients with COVID-2019. Nature doi:10.1038/s41586-020-2196-x.
6. WHO. 2020. Report of the WHO-China Joint Mission on Coronavirus Disease 2019 (COVID-19). <https://wwwwhoint/docs/default-source/coronaviruse/who-china-joint-mission-oncovid-19-final-reportpdf>
7. Anand K, Palm GJ, Mesters JR, Siddell SG, Ziebuhr J, Hilgenfeld R. 2002. Structure of coronavirus main proteinase reveals combination of a chymotrypsin fold with an extra alpha-helical domain. EMBO J 21:3213-24.
8. Sisay M. 2020. 3CL(pro) inhibitors as a potential therapeutic option for COVID-19: Available evidence and ongoing clinical trials. Pharmacol Res doi:10.1016/j.phrs.2020.104779:104779.
9. Liu C, Zhou Q, Li Y, Garner LV, Watkins SP, Carter LJ, Smoot J, Gregg AC, Daniels AD, Jervey S, Albaiu D. 2020. Research and Development on Therapeutic Agents and Vaccines for COVID-19 and Related Human Coronavirus Diseases. ACS Cent Sci 6:315-331.
10. Wu CJ, Jan JT, Chen CM, Hsieh HP, Hwang DR, Liu HW, Liu CY, Huang HW, Chen SC, Hong CF, Lin RK, Chao YS, Hsu JT. 2004. Inhibition of severe acute respiratory syndrome coronavirus replication by niclosamide. Antimicrob Agents Chemother 48:2693-6.
11. Hung HC, Tseng CP, Yang JM, Ju YW, Tseng SN, Chen YF, Chao YS, Hsieh HP, Shih SR, Hsu JT. 2009. Aurintricarboxylic acid inhibits influenza virus neuraminidase. Antiviral Res 81:123-31.
12. Hatada R, Okuwaki K, Mochizuki Y, Handa Y, Fukuzawa K, Komeiji Y, Okiyama Y, Tanaka S. 2020. Fragment Molecular Orbital Based Interaction Analyses on COVID-19 Main Protease - Inhibitor N3 Complex (PDB ID: 6LU7). J Chem Inf Model doi:10.1021/acs.jcim.0c00283.
13. Venkatachalam CM, Jiang X, Oldfield T, Waldman M. 2003. LigandFit: a novel method for the shape-directed rapid docking of ligands to protein active sites. Journal of Molecular Graphics & Modelling 21:289-307.
14. Kankanamalage ACG, Kim Y, Damalanka VC, Rathnayake AD, Fehr AR, Mehzabeen N, Battaile KP, Lovell S, Lushington GH, Perlman S, Chang KO, Groutas WC. 2018. Structure-guided design of potent and permeable inhibitors of MERS coronavirus 3CL protease that utilize a piperidine moiety as a novel design element. European Journal of Medicinal Chemistry 150:334-346.
15. Gawehn E, Hiss JA, Schneider G. 2016. Deep Learning in Drug Discovery. Mol Inform 35:3-14.
16. Kuo CJ, Chi YH, Hsu JT, Liang PH. 2004. Characterization of SARS main protease and inhibitor assay using a fluorogenic substrate. Biochem Biophys Res Commun 318:862-7.
17. Hsu JT, Kuo CJ, Hsieh HP, Wang YC, Huang KK, Lin CP, Huang PF, Chen X, Liang PH. 2004. Evaluation of metal-conjugated compounds as inhibitors of 3CL protease of SARS-CoV. FEBS Lett 574:116-20.
18. Kim Y, Lovell S, Tiew KC, Mandadapu SR, Alliston KR, Battaile KP, Groutas WC, Chang KO. 2012. Broad-spectrum antivirals against 3C or 3C-like proteases of picornaviruses, noroviruses, and coronaviruses. J Virol 86:11754-62.
19. St John SE, Therkelsen MD, Nyalapatla PR, Osswald HL, Ghosh AK, Mesecar AD. 2015. X-ray structure and inhibition of the feline infectious peritonitis virus 3C-like protease: Structural implications for drug design. Bioorg Med Chem Lett 25:5072-7.

20. Cao B, Wang Y, Wen D, Liu W, Wang J, Fan G, Ruan L, Song B, Cai Y, Wei M, Li X, Xia J, Chen N, Xiang J, Yu T, Bai T, Xie X, Zhang L, Li C, Yuan Y, Chen H, Li H, Huang H, Tu S, Gong F, Liu Y, Wei Y, Dong C, Zhou F, Gu X, Xu J, Liu Z, Zhang Y, Li H, Shang L, Wang K, Li K, Zhou X, Dong X, Qu Z, Lu S, Hu X, Ruan S, Luo S, Wu J, Peng L, Cheng F, Pan L, Zou J, Jia C, Wang J, Liu X, Wang S, Wu X, Ge Q, He J, Zhan H, Qiu F, Guo L, Huang C, Jaki T, Hayden F. G., Horby P. W., Zhang D, Wang C. 2020. A Trial of Lopinavir-Ritonavir in Adults Hospitalized with Severe Covid-19. N Engl J Med 382:1787-1799.

21. Hsieh HP, Wang WC, Shiao HY, Ke YY, Lin WH, Hsu JTA, Chen CT, Yeh TK. 2017. Discovery of BPR1K871-a quinazoline based multi-kinase inhibitor for the treatment of AML and solid tumors: Rational design, synthesis, in vitro and in vivo evaluation. Abstracts of Papers of the American Chemical Society 253.

22. Shiao HY, Coumar MS, Chang CW, Ke YY, Chi YH, Chu CY, Sun HY, Chen CH, Lin WH, Fung KS, Kuo PC, Huang CT, Chang KY, Lu CT, Hsu JTA, Chen CT, Jiaang WT, Chao YS, Hsieh HP. 2013. Optimization of Ligand and Lipophilic Efficiency To Identify an in Vivo Active Furano-Pyrimidine Aurora Kinase Inhibitor. Journal of Medicinal Chemistry 56:5247-5260.

23. Cournia Z, Allen B, Sherman W. 2017. Relative Binding Free Energy Calculations in Drug Discovery: Recent Advances and Practical Considerations. Journal of Chemical Information and Modeling 57:2911-2937.

24. Hussey RJ, Coates L, Gill RS, Erskine PT, Coker SF, Mitchell E, Cooper JB, Wood S, Broadbridge R, Clarke IN, Lambden PR, Shoolingin-Jordan PM. 2011. A structural study of norovirus 3C protease specificity: binding of a designed active site-directed peptide inhibitor. Biochemistry 50:240-9.

25. Colson P, Rolain JM, Raoult D. 2020. Chloroquine for the 2019 novel coronavirus SARS-CoV-2. Int J Antimicrob Agents 55:105923.

26. Gautret P, Lagier JC, Parola P, Hoang VT, Meddeb L, Mailhe M, Doudier B, Courjon J, Giordanengo V, Vieira VE, Dupont HT, Honore S, Colson P, Chabriere E, La Scola B, Rolain JM, Brouqui P, Raoult D. 2020. Hydroxychloroquine and azithromycin as a treatment of COVID-19: results of an open-label non-randomized clinical trial. Int J Antimicrob Agents doi:10.1016/j.ijantimicag.2020.105949:105949.

27. Lei J, Hilgenfeld R. 2017. RNA-virus proteases counteracting host innate immunity. FEBS Lett 591:3190-3210.

28. Hung HC, Wang HC, Shih SR, Teng IF, Tseng CP, Hsu JT. 2011. Synergistic inhibition of enterovirus 71 replication by interferon and rupintrivir. J Infect Dis 203:1784-90.

29. Tiew KC, He G, Aravapalli S, Mandadapu SR, Gunnam MR, Alliston KR, Lushington GH, Kim Y, Chang KO, Groutas WC. 2011. Design, synthesis, and evaluation of inhibitors of Norwalk virus 3C protease. Bioorg Med Chem Lett 21:5315-9.

30. Mandadapu SR, Weerawarna PM, Gunnam MR, Alliston KR, Lushington GH, Kim Y, Chang KO, Groutas WC. 2012. Potent inhibition of norovirus 3CL protease by peptidyl alpha-ketoamides and alpha-ketoheterocycles. Bioorg Med Chem Lett 22:4820-6.

31. Kim Y, Liu H, Galasiti Kankanamalage AC, Weerasekara S, Hua DH, Groutas WC, Chang KO, Pedersen NC. 2016. Reversal of the Progression of Fatal Coronavirus Infection in Cats by a Broad-Spectrum Coronavirus Protease Inhibitor. PLoS Pathog 12:e1005531.

408 **Table 1. Inhibitory activity of HIV protease inhibitors on SARS-CoV-2 M^{pro}.**

409

Compounds	Activity
Lopinavir , Ritonavir, Fosamprenavir, Saquinavir, Nelfinavir, Atazanavir, Darunavir, Amprenavir, Tipranavir, Indinavir	No one has activity at 20 μM.

410

411

Antimicrobial Agents and Chemotherapy

Figure 1

(A)

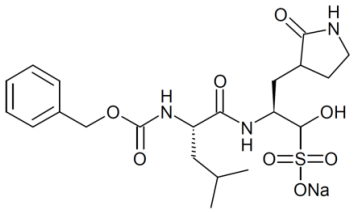

(B)

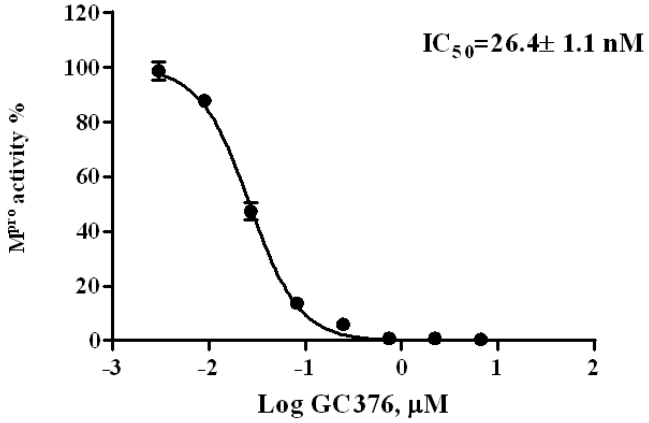

(C)

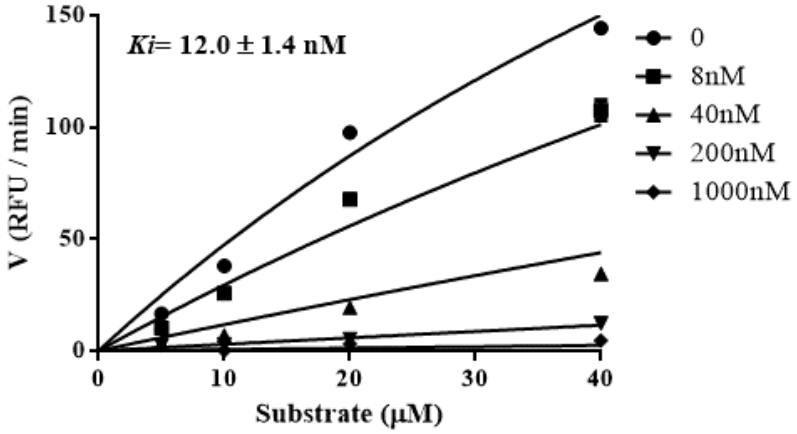

Figure 2

(A)

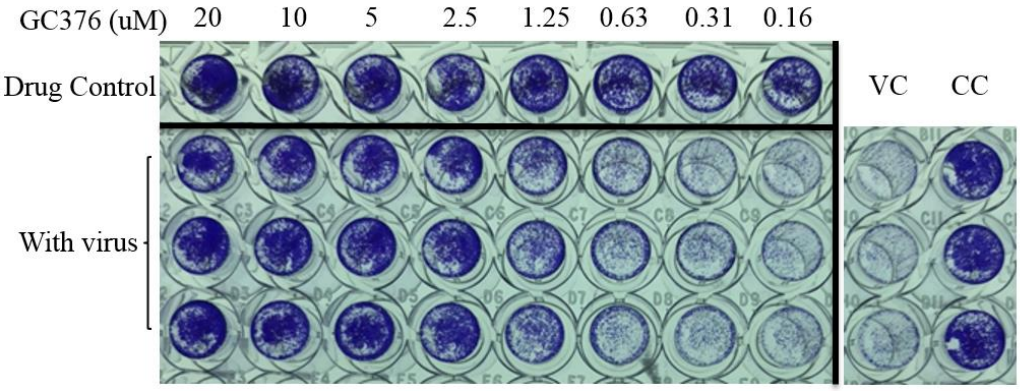

(B)

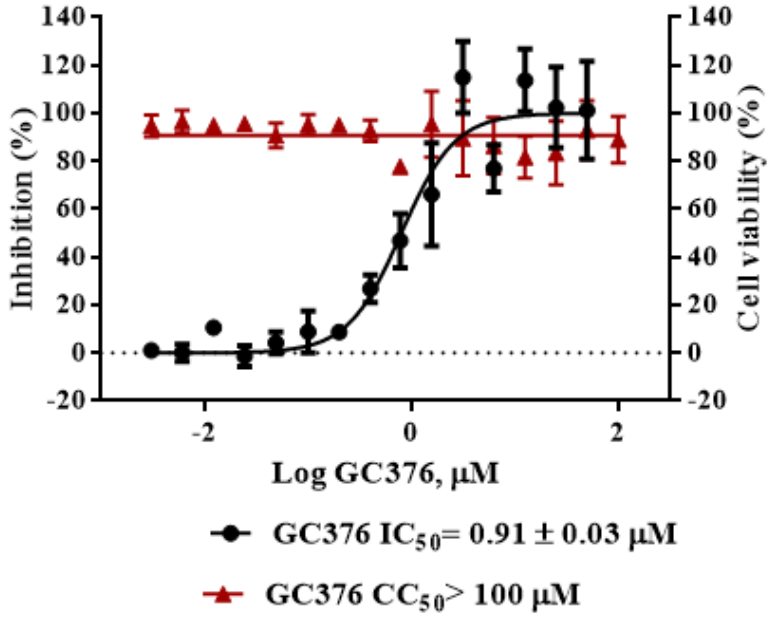

Figure 3

(A) GC376 docking to SARS-CoV-2 main protease (M^{pro}) x-ray structure (PDBID: 6LU7)

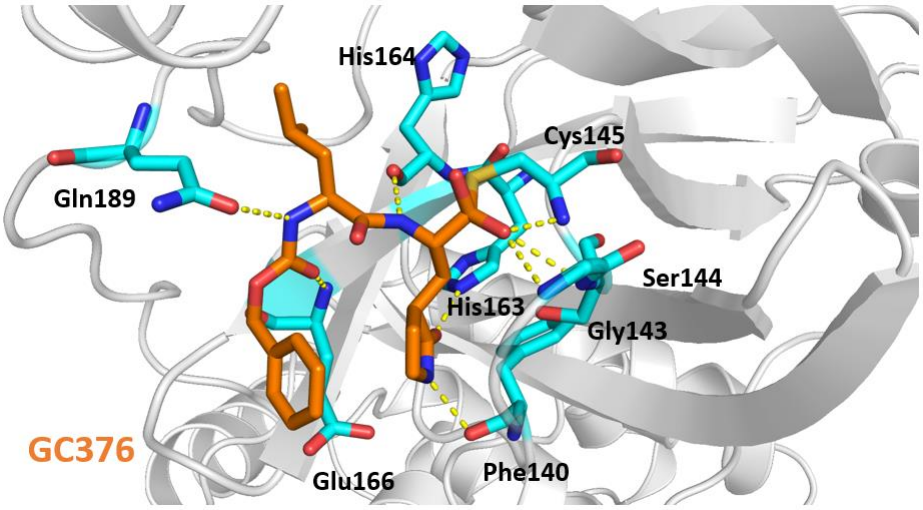

(B) GC376 docking to FIPV main protease (M^{pro}) x-ray structure (PDBID: 4ZRO)

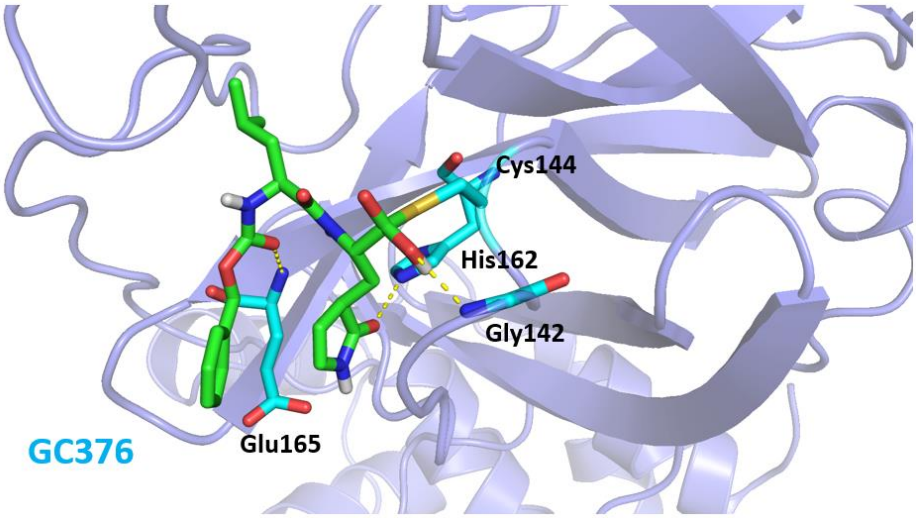

441 (C)
442

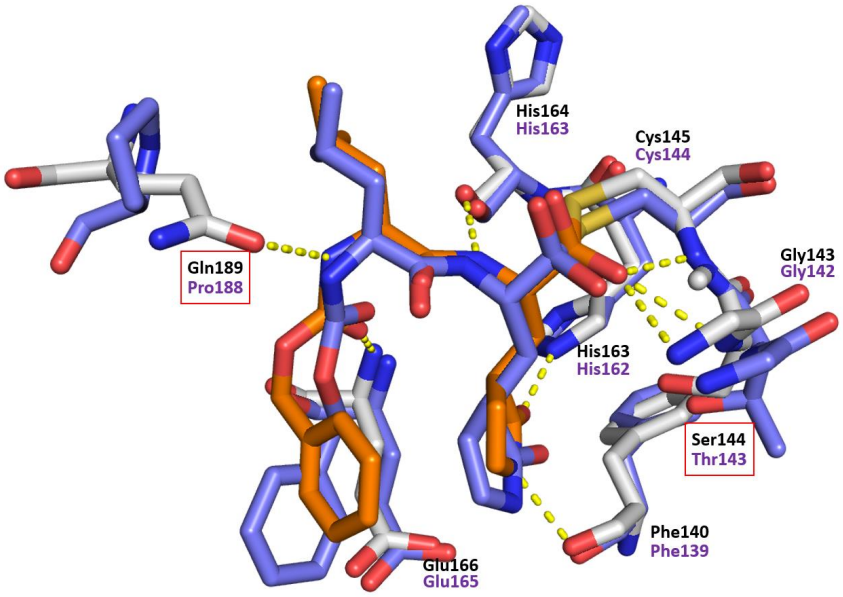

443
444

Figure Legends

Fig.1. Structure of GC376 and the IC_{50} and the inhibitory constant (Ki) of recombinant M^{pro} of SARS-CoV-2. (A) GC376 is a peptidomimetic antiviral drug. (B) The IC_{50} and the inhibitory constant (*Ki*) of M^{pro} of SARS-CoV-2. The proteolytic activity of M^{pro} was determined by the FRET protease assay as described.

Fig. 2. GC376 inhibited SARS-CoV-2 virus replication in Vero E6 cells. (A) The inhibition of SARS-CoV-2-induced CPE by GC376. In 96-well plate, Vero E6 cells were infected with SARS-CoV-2 virus (100 $TCID_{50}$ per well) and cells were treated with various concentrations of GC376. At 120 h post-infection (*hpi*), cells were examined by a microscope (100×). Cell control: normal cells without treatment; Virus: cells infected with SARS-CoV-2 virus at 100 $TCID_{50}$/well; in the absence or presence of GC376 at 0.39, 0.78 or 1.56 μM, respectively. (B) Viable cells were stained with crystal violet. Results from one representative plate of two are shown. (C) Effects of GC376 on SARS-CoV-2-induced CPE or cell proliferation were generated using a sigmoidal dose-response curve model (GraphPad Prism 6 software) from which the IC_{50} values were derived. The effect of GC376 on cell proliferation was determined by MTT assay.

Fig. 3. Docked conformations of GC376 in SARS-CoV-2 and FIPV M^{pro} proteases. (a) GC376 docking to SARS-CoV-2 M^{pro} protein x-ray structure (PDBID: 6LU7). (b) GC376 docking to FLIP 3C-like protease protein x-ray structure (PDBID: 4ZRO). (c) Structure alignment of FIPV (PDB ID: 4ZRO, purple) and SARS-CoV-2 (PDB ID: 6LU7, White). The docking result of GC376 in FIPV is display as cyan, and docking result of GC376 in is display as orange. The red box shows the difference residues in the FIPV and SARS-CoV-2 binding site.